# Multistate Electron Transfer Dynamics in the Condensed Phase: Numerically Exact Calculations from the Reduced Hierarchy Equations of Motion Approach

Midori Tanaka

*Theoretical Chemistry Group*

*Department of Chemistry, Graduate School of Science,*
*Kyoto University*
*Kyoto 606-8502, Japan*

January 29, 2010

## Acknowledgements

The works described in the thesis have been performed under the supervision of Professor Yoshitaka Tanimura. The author would like to express her sincere gratitude to Professor Tanimura for his guidance and encouragement. The author is grateful to Professor Akira Yoshimori (Kyushu University), Dr. Arend G. Dijkstra, and Dr. Hirotaka Nishioka for fruitful discussion. The author would like to thank all members of the laboratory for helps and useful comments.

## Abstract

Multiple displaced oscillators coupled to an Ohmic heat-bath are used to describe electron transfer (ET) in a dissipative environment. By performing a canonical transformation, the model is reduced to a multi-level system coupled to a heat-bath with the Brownian spectral distribution. A reduced hierarchy equations of motion approach is introduced for numerically rigorous simulation of the dynamics of the three-level system with various oscillator configurations, for different nonadiabatic coupling strengths and damping rates, and at different temperatures. The time evolution of the reduced density matrix elements illustrates the interplay of coherences between the electronic and vibrational states. The ET reaction rates, defined as a flux-flux correlation function, are calculated using the linear response of the system to an external perturbation as a function of activation energy. The results exhibit an asymmetric inverted parabolic profile in a small activation regime due to the presence of the intermediate state between the reactant and product states and a slowly decaying profile in a large activation energy regime, which arises from the quantum coherent transitions.

## List of Publications

1. M. Tanaka and Y. Tanimura:

   *Quantum Dissipative Dynamics of Electron Transfer Reaction System: Nonperturbative Hierarchy Equations Approach*

   Journal of the Physical Society of Japan, Vol. 78, 073802(2009)

2. M. Tanaka and Y. Tanimura:

   *Multistate Electron Transfer Dynamics in the Condensed Phase: Exact Calculations from the Reduced Hierarchy Equations of Motion Approach*

   (Submitted to the Journal of Chemical Physics)

# Contents

# List of Figures

# Chapter 1

# Introduction

The analysis of electron transfer (ET) processes is of great interest to a variety of researches in chemistry, biology, and physics.[1, 2, 3, 4, 5] Most ET processes occur in condensed phases where the surrounding molecules provide the fluctuations and dissipation needed in the reactions.[6, 7, 8, 9, 10] In a widely used model for ET problems, the electronic states are coupled to an intermediate harmonic nuclear or intramolecular vibrational mode, which is in turn coupled to a heat-bath.[11, 12] This model describes fundamental chemical rate processes, interactions of a molecule with a dissipative and fluctuating environment,[7] and Marcus theory for non-adiabatic electron transfer.[4] Further extensions of the model are used in laser spectroscopy to describe the coupling of electronic states to vibrational modes[13] and the coupling of electronic states in solids to phonons.[14] By adopting this description, one may study ET processes by nonlinear optical measurements with, for example, correlation function formalism based on the Liouville-space semiclassical propagation scheme,[15, 16, 17] the diffusion-reaction equation method,[18] the multistate quantum Fokker-Planck approach,[19, 20, 21] or the multilevel

Redfield theory.[22, 23, 24] Tremendous insight was gained from this model from quantitative analytical calculations[25, 26, 11, 12, 27, 28, 29, 30, 31, 32, 33, 34, 35, 36] and numerical studies[37, 38, 19, 20, 21, 39, 40, 41, 42, 43, 44, 45, 46, 47, 48, 49, 50, 25, 51, 52, 53, 26, 22, 23, 24, 54, 55, 56] stimulated by experiments.[57, 58, 59, 60, 61, 62, 63, 18, 64]

Many aspects have been discussed individually under some limited regime. In any approach, the full quantum treatment poses some difficult problems. While quantum nonadiabatic transitions in the absence of the bath can be studied by a wide variety of numerical methods based on the wavefunction,[65] a reduced density operator has to be used in the presence of the bath in order to study the irreversibility of system dynamics toward the thermal equilibrium state.[66]

In the ET case, the harmonic mode of a nuclear or an intramolecular vibration can be included in the bath by carrying out a canonical transformation, which leads to a multi-level system coupled to the heat-bath with the canonically transformed spectral distribution function.[11] Then the reduction of the bath degrees of freedom can be performed using projection operator or path integral techniques.

While the projection operator approach and path integral approach are formally exact,[67, 68] one has to employ some approximation to derive reduced equation of motion such as the multilevel Redfield equation,[37, 22, 23, 24] the mixed quantum-classical equations of motion,[25, 26] and stochastic Liouville equations[38, 39, 42, 43, 44, 45] which can be solved numerically. The master equation approach requires several crucial assumptions,

such as the rotating wave approximation, the white noise (or Van Hove) approximation, and the factorized initial condition. These approximations strongly limit the equation's applicability especially at a low temperature, where quantum effects play a major role. Time convolution-less master and Redfield equations have a wider range of applicability; however, because both equations depend upon the factorization assumption, they cannot be applied to calculate the nonlinear response of the system dynamics arising from time-dependent external perturbations.[69]

The path integral approach, where the reduced density matrix elements are expressed in terms of the nonadiabatic interactions in functional form, is powerful for a strong system-bath coupling.[11, 12, 27, 28, 29] However, since this approach handles nonadiabatic coupling perturbatively, it is not easy to study strong nonadiabatic (diabatic) coupling. Path integral Monte Carlo simulations can remove this limitation, but their applicability is limited because of the sampling processes.[40, 41] Note that the linear and nonlinear optical response functions obtained from cumulant expansion approaches have a similar form as the perturbative results from path integrals, since laser interactions play a similar role as the nonadiabatic coupling. [15, 16, 17]

To eliminate all of the above mentioned limitations, one can derive the hierarchy equations of motion for the reduced density matrix by differentiating the reduced density matrix elements defined by path integrals.[66] This approach was first introduced to investigate the connection between the phenomenological stochastic Liouville equation theory and the dynamical Hamiltonian theory, and was limited to the case in which the spec-

tral distribution function is given by the Drude form (Ohmic form with a Lorentzian cutoff) and the bath temperature is relatively high.[70] By including low temperature corrections terms, the temperature limitation can be eliminated.[71, 72, 73, 66, 74] This formalism is valuable since it can handle not only the strong system-bath coupling but also quantum coherence between the system and bath which plays an important role for the electronic energy transfer (EET) in photosynthetic antenna system.[75, 76]

Although the form of hierarchy becomes complicated, it is possible to derive the hierarchy equations of motion for nonOhmic spectral distributions.[71] If one applies the hierarchy formalism to the Brownian spectral distribution that arises from the canonical transformation of ET system, one can handle the ET problem in a nonperturbative manner for both the system-bath and nonadiabatic couplings.[19] While the previously derived hierarchy equations for a two-state ET system cannot be applied to a low-temperature system, where the quantum transition plays a major role, we can remove this limitation by introducing the low temperature correction terms for the Brownian spectral distribution hierarchy.[77] Moreover, we can formulate the equations of motion for a multistate system, where the interplay between the sequential and super-exchange ET transitions[1] becomes important.[30, 40, 32, 33, 34,

[1]The ET process of the three-state electronic system is often depicted in terms of the sequential mechanism and the super-exchenge. When the free energy of the intermediate state is close to or lower than the thermal energy $k_BT$, the ET occurs by the sequential mechanism, in which the ET from the intermediate state to the final takes place after the thermalization of phonons in the intermediate state. On the other hand, when the free energy of the intermediate state is much higher than $k_BT$, the ET occurs unistep from the initial state to the final by the super-exchange mechanism, in which the intermediate state is passed as a quantum mechanical virtual state.[32, 33, 34, 35, 36, 62]

35, 36, 31]

A typical example of three-state problem is bacterial photosynthesis where the ET takes place between the excited special pair to the bacteriopheophytin mediated by the accessory chlorophylI monomer stationed in between them.[78] Many experimental and theoretical studies have carried out to explore the mechanism of the primary ET step in photosynthetic bacteria. [58, 59, 60, 61, 41, 32, 33, 34]

In this paper, we present a complete study of the various nonperturbative regimes of electron transfer processes, using the hierarchy of quantum kinetic equations. The present numerical study allows us to demonstrate a number of the features arising from the interplay between quantum nonadiabatic transition and dissipation. The organization of this paper is as follows: the model Hamiltonian and canonical transformed Hamiltonian are presented in the chapter 2. In the chapter 3 the hierarchy equations of motion for Brownian spectral distribution with low temperature correction terms is presented. Time evolution of a three-state system is studied by numerically solving the hierarchy equations over wide parameter ranges in the chapter 4. The ET rates as the function of temperature and activation energy are presented and discussed in the chapter 5. The last chapter is devoted to concluding remarks.

# Chapter 2

# The Model

We consider the case that the electronic energy states depend on nuclear configuration. The simplified model for this is harmonic oscillators system displaced along a reaction coordinate with different excitation energies (see Fig. 2.1).

We denote the coordinate, momentum, mass and frequency of the single harmonic mode by $Q$, $P$, $M$, and $\omega_0$, respectively. To distinguish from the bath mode, hereafter we refer this mode as the ($P$, $Q$) oscillator mode. In this paper, we limit our analysis to the three-state case, since the extensions to more than four states are straightforward. The oscillator states further coupled to the bath state represented by an ensemble of harmonic oscillators. A commonly used model for ET problems is then expressed as[11, 12]

$$\begin{aligned} \hat{H} &= \hat{H}_A - \sum_{j=1}^{3} M\omega_0^2 Q d_j D|j\rangle\langle j| + \frac{P^2}{2M} + \frac{1}{2}M\omega_0^2 Q^2 \\ &\quad + \sum_{\alpha}^{\infty} \left\{ \frac{p_\alpha^2}{2m_\alpha} + \frac{1}{2}m_\alpha\omega_\alpha^2 \left( x_\alpha - \frac{c_\alpha}{m_\alpha\omega_\alpha^2} Q \right)^2 \right\}, \end{aligned} \tag{2.1}$$

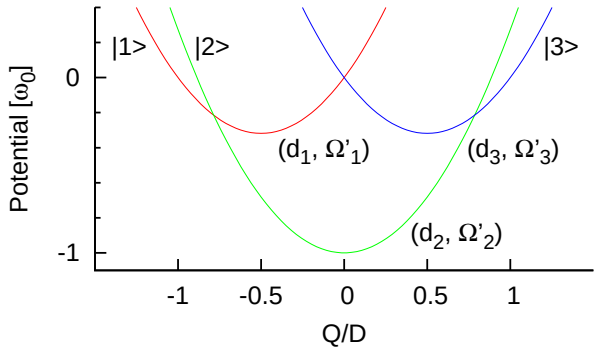


Figure 2.1: Schematic view of a three-state system coupled to a harmonic mode. The parabolic potential for the state $|j\rangle$ has the vertex $(d_j, \Omega'_j)$, where $\Omega'_j = \Omega_j - \lambda d_j^2$. The red, green, and blue lines are for the $|1\rangle$, $|2\rangle$, and $|3\rangle$ states, respectively. Here, parameters are the same as at the beginning of the chapter 3.

where the system Hamiltonian is defined by

$$\hat{H}_A = \sum_{j=1}^{3} \hbar\Omega_j |j\rangle\langle j| + \sum_{j=1,k\neq j}^{3} \hbar\Delta_{jk} |j\rangle\langle k|. \tag{2.2}$$

Here, $\hbar\Omega_j$ is energy of the electronic state $|j\rangle$, and $\hbar\Delta_{j,k}$ is the transfer coupling between the $j$ and $k$-th states, and $d_j D$ represents the displacement of the $(P, Q)$ oscillator for $|j\rangle$, where $D$ is the characteristic length of the system. $x_\alpha$, $p_\alpha$, $m_\alpha$, and $\omega_\alpha$ denote the coordinate, momentum, mass and frequency of the bath mode $\alpha$. The constant $c_\alpha$ is the coupling strength to the mode $\alpha$. The character of the bath is determined by the spectral distribution function $J(\omega) = \sum_\alpha^\infty c_\alpha^2 \delta(\omega - \omega_\alpha)/(2m_\alpha\omega_\alpha)$. Here we consider the Ohmic case that is defined by $J(\omega) = M\gamma\omega$.

By performing the canonical transformation,[11] the Hamiltonian of this model is converted to that of the three-state system directly coupled to a bath

of infinite harmonic oscillators with a significantly different bath spectral density,[77]

$$\hat{H} = \hat{H}_A - \hat{V}\sum_{\alpha}^{\infty} c'_\alpha x'_\alpha + \sum_{\alpha}^{\infty}\left(\frac{p'^2_\alpha}{2m'_\alpha} + \frac{1}{2}m'_\alpha \omega'^2_\alpha x'^2_\alpha\right), \tag{2.3}$$

where the system-bath coupling $\hat{V}$ is written as

$$\hat{V} = \sum_{j=1}^{3} d_j |j\rangle\langle j|, \tag{2.4}$$

and $x'_\alpha$, $p'_\alpha$, $m'_\alpha$, $\omega'_\alpha$, and $c'_\alpha$ are the transformed $\alpha$-th coordinate, momentum, mass, frequency, and the coupling strength, respectively. The spectral distribution function $J(\omega) = \sum_\alpha^\infty c'^2_\alpha \delta(\omega - \omega'_\alpha)/(2m'_\alpha\omega'_\alpha)$ is also transformed as[11]

$$J(\omega) = \frac{2\hbar\lambda}{\pi}\cdot\frac{\gamma\omega_0^2\omega}{(\omega_0^2-\omega^2)^2+\gamma^2\omega^2}, \tag{2.5}$$

where $\lambda = MD^2\omega_0^2/2\hbar$ with the fixed $D$. We refer the above spectral distribution as the Brownian form since it arises from the correlation function of the Brownian oscillator system (see Appendix A).[27, 29, 28] The distribution is characterized by the characteristic frequency $\omega_0$, the displacement $\lambda$, and the coupling strength between the ($P$, $Q$) oscillator and the bath $\gamma$ and the peak position and the peak width of $J(\omega)$ change with $\gamma$ (see Fig. 2.2).

If the potential surface of the ($P$, $Q$) mode are anharmonic, one has to explicitly deal with the ($P$,$Q$) degrees of freedom by employing the multi-state descriptions of the quantum kinetic equation[20, 21] or semi-classical kinetic equation.[25, 39, 26] However, if the ($P$, $Q$) potential is harmonic, we can reduce the ($P$, $Q$) degrees of freedom into the bath, which allows us to simplify the ET problem and to save the CPU power dramatically. This

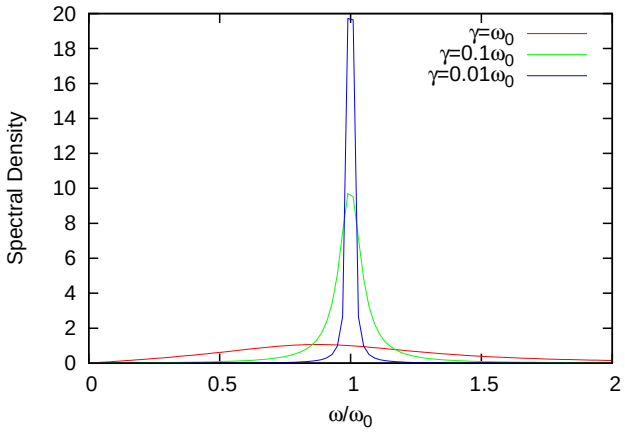


Figure 2.2: The normalized spectral density $J(\omega)\pi/(2\hbar\lambda)$ for $\gamma = \omega_0$ (red line), $0.1\omega_0$ (green line), and $0.01\omega_0$ (blue line). The peak position and the peak width of $J(\omega)\pi/(2\hbar\lambda)$ change with $\gamma$.

simplification is necessary to handle the multi-dimensional hierarchy arising from the low-temperature correction terms.[71, 72, 73, 66, 74]

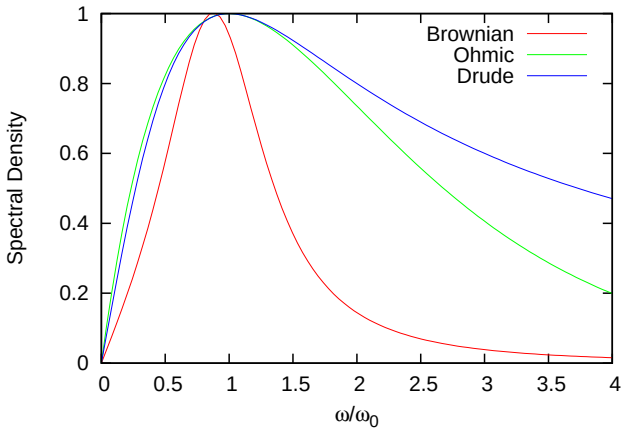


Figure 2.3: Comparison between the Brownian spectral density, the Ohmic case with an exponential cutoff (the Ohmic spectral density), and that with a Lorentzian cutoff (the Drude spectral densiry). The spectral densities $J(\omega)$ in a case of $\gamma = \omega_0$ (red line) for the Brownian spectral density, $J_O(\omega) = \eta_O \omega \exp[-\omega/\omega_0]/\omega_0$ (green line) for the Ohmic spectral density, and $J_D(\omega) = \eta_D \omega\omega_0/(\omega_0^2 + \omega^2)$ (blue line) for the Drude spectral density. Here $\eta_O$ and $\eta_D$ are the coupling constants and we set the maximum values of $J(\omega)$, $J_O(\omega)$, and $J_D(\omega)$ are the same (1).

# Chapter 3

# Hierarchy Equations of Motion for the Reduced Density Matrix Elements

The reduced density matrix of this system can be treated by the path-integral formalism by utilizing the coherent state representation.[79] While the conventional coherent state representation is for two-state system,[70, 80] here we extend it for three-state as $|\psi\rangle = |0\rangle + |1\rangle\phi_1 + |2\rangle\phi_1\phi_2$, where $\phi$ is a Grassmann number. Since $|\psi\rangle$ is not orthogonal, the completeness relation is then expressed as

$$\begin{aligned} &\int d\bar{\psi}d\psi|\psi\rangle\langle\psi|e^{-\bar{\phi_1}\bar{\phi_2}\phi_1\phi_2-\bar{\phi_2}\phi_2} \\ &\equiv \int d\bar{\phi_1}d\bar{\phi_2}d\phi_2 d\phi_1|\psi\rangle\langle\psi|e^{-\bar{\phi_1}\bar{\phi_2}\phi_1\phi_2-\bar{\phi_2}\phi_2} \\ &= 1, \end{aligned} \tag{3.1}$$

where $\langle\psi| = \langle 0| + \bar{\phi_2}\langle 1| + \bar{\phi_2}\bar{\phi_1}\langle 2|$. Hereafter $\psi$ represents a set of two Grassmann numbers $\{\phi_1, \phi_2\}$. The following procedure to derive the equation of motion is parallel to that in the high-temperature Drude distribution case.[70]

In order to have the reduced density matrix elements in a compact form, we employ a temporary initial condition of the total system in the factorized form as $\hat{\rho}_A(t_0) \otimes \hat{\rho}_B^{eq}$, where $\hat{\rho}_B^{eq}$ is the equilibrium density matrix of the bath. This assumption can be removed once we derive the equations of motion by setting $t_0 \ll -\Omega_c$ and by integrating up to time the $t = 0$, where $\Omega_c$ is characteristic relaxation time of the system, to have the correlated initial condition at $t = 0$.[66]

The reduced density matrix element is expressed in the path integral form as

$$\begin{aligned} \rho(\bar{\psi}, \psi'; t) &= \int D[\psi(\tau)] D[\bar{\psi}(\tau)] D[\psi'(\tau)] D[\bar{\psi}'(\tau)] \\ &\quad \times \mathrm{e}^{iS_A[\bar{\psi},\psi]/\hbar} F[\bar{\psi}, \psi, \bar{\psi}', \psi'; t] \mathrm{e}^{-iS_A[\bar{\psi}',\psi']/\hbar}, \end{aligned} \tag{3.2}$$

where $\int D[\psi(\tau)]$ represents the functional integral of a set of Grassmann variables $\psi = \{\phi_1, \phi_2\}$ which describe the three of the system states. The action for the system's Hamiltonian Eq. (2.2) is denoted by $S_A[\bar{\psi}, \psi]$. Feynman-Vernon influence functional which describes the bath effects is denoted by $F[\bar{\psi}, \psi, \bar{\psi}', \psi'; t]$.[81, 68]

The bath degrees of freedom can be reduced by performing the path integrals for the coordinate $x'_\alpha$, which leads to the influence functional in the form[68]

$$\begin{aligned} F[\bar{\psi}, \psi, \bar{\psi}', \psi'; t] &= \exp\left[ -\frac{1}{\hbar} \int_{t_0}^{t} ds \int_{t_0}^{s} du V^{\times}(s) \right. \\ &\quad \left. \times \left( -iL_1(s-u) V^{\circ}(u) + L_2(s-u) V^{\times}(u) \right) \right], \end{aligned} \tag{3.3}$$

where $V^{\times}(t) \equiv V(\bar{\psi}(t), \psi(t)) - V(\bar{\psi}'(t), \psi'(t))$ and $V^{\circ}(t) \equiv V(\bar{\psi}(t), \psi(t)) + V(\bar{\psi}'(t), \psi'(t))$ are the commutator and anticommutator of $\hat{V}$ expressed in

the coherent state representation of sets of Grassmann numbers. The time-dependent kernels corresponding to the dissipation $L_1(t) \equiv \langle [Q(t), Q] \rangle / \hbar$ and fluctuation $L_2(t) \equiv \langle Q(t)Q + QQ(t) \rangle / 2\hbar$ induced by the bath are expressed by the spectral distribution as

$$L_1(t) = \int_0^\infty d\omega J(\omega) \sin(\omega t) \tag{3.4}$$

and

$$L_2(t) = \int_0^\infty d\omega J(\omega) \coth(\beta\hbar\omega/2) \cos(\omega t), \tag{3.5}$$

respectively.[66, 70, 68] For eq. (2.5), we have

$$L_1(t) = \frac{\hbar\lambda\omega_0^2}{2i\zeta} \left\{ \mathrm{e}^{-\left(\frac{\gamma}{2} - i\zeta\right)t} - \mathrm{e}^{-\left(\frac{\gamma}{2} + i\zeta\right)t} \right\} \tag{3.6}$$

and

$$\begin{aligned} L_2(t) &= -\frac{4\lambda\gamma\omega_0^2}{\beta} \sum_{k=1}^{\infty} \frac{\nu_k}{(\omega_0^2 + \nu_k^2)^2 - \gamma^2\nu_k^2} \mathrm{e}^{-\nu_k t} \\ &\quad + \frac{\hbar\lambda\omega_0^2}{2\zeta} \mathrm{e}^{-(\frac{\gamma}{2} - i\zeta)t} \coth\left( \frac{\beta\hbar}{2} \left( \zeta + i\frac{\gamma}{2} \right) \right) \\ &\quad - \frac{\hbar\lambda\omega_0^2}{2\zeta} \mathrm{e}^{-(\frac{\gamma}{2} + i\zeta)t} \coth\left( \frac{\beta\hbar}{2} \left( -\zeta + i\frac{\gamma}{2} \right) \right), \end{aligned} \tag{3.7}$$

where $\zeta = \sqrt{\omega_0^2 - \gamma^2/4}$ for $\gamma < 2\omega_0$ and $\nu_k = (2\pi/\beta\hbar)k$ with $2\pi/\beta\hbar$ being the Matsubara frequency. Submitting Eqs. (3.6) and (3.7) into Eq. (3.8) and rearranging terms, we can express the influence functional as[77]

$$\begin{aligned} F[\bar{\psi}, \psi, \bar{\psi}', \psi'; t] &= \exp\left[ -\int_{t_0}^t ds \int_{t_0}^s du V^\times(s) \right. \\ &\quad \left. \times \left( \Theta_-(u) \mathrm{e}^{-(\frac{\gamma}{2} - i\zeta)(s-u)} + \Theta_+(u) \mathrm{e}^{-(\frac{\gamma}{2} + i\zeta)(s-u)} \right) \right] \\ &\quad \times \exp\left[ \int_{t_0}^t ds \int_{t_0}^s du V^\times(s) \sum_{k=1}^{\infty} \Psi_k(u) \nu_k \mathrm{e}^{-\nu_k(s-u)} \right] \end{aligned} \tag{3.8}$$

where

$$\Theta_{\pm}(u) = \frac{\lambda\omega_0^2}{2\zeta}\left\{\pm\coth\left[\frac{\beta\hbar}{2}\left(\mp\frac{\zeta}{2}+i\frac{\gamma}{2}\right)\right]V^{\times}(u)\mp V^{\circ}(u)\right\}, \tag{3.9}$$

and

$$\Psi_k(u) = \frac{4\lambda}{\beta\hbar}\frac{\gamma\omega_0^2}{(\omega_0^2+\nu_k^2)^2-\gamma^2\nu_k^2}V^{\times}(u). \tag{3.10}$$

If we choose $K$ so as to satisfy

$$\nu_K = \frac{2\pi}{\beta\hbar}K \gg \max\{\Omega_l-\Omega_m\}_{l,m}, \tag{3.11}$$

the function $\mathrm{e}^{-\nu_k(s-u)}$ for $k \geq K$ in Eq. (3.8) can be replaced by Dirac's delta function $\nu_k\mathrm{e}^{\nu_k(s-u)} \simeq \delta(s-u)$. This leads the influence functional Eq. (3.8) to

$$\begin{aligned}
F[\bar{\psi},\psi,\bar{\psi}',\psi';t] \simeq& \exp\left[-\int_{t_0}^{t}ds\int_{t_0}^{s}duV^{\times}(s)\right.\\
&\left.\times\left(\Theta_{-}(u)\mathrm{e}^{-(\frac{\gamma}{2}-i\zeta)(s-u)}+\Theta_{+}(u)\mathrm{e}^{-(\frac{\gamma}{2}+i\zeta)(s-u)}\right)\right]\\
&\times\exp\left[\int_{t_0}^{t}ds\int_{t_0}^{s}duV^{\times}(s)\sum_{k=1}^{K}\Psi_k(u)\nu_k\mathrm{e}^{-\nu_k(s-u)}\right]\\
&\times\exp\left[\int_{t_0}^{t}ds\Xi(s)\right],
\end{aligned} \tag{3.12}$$

where

$$\Xi(s) = V^{\times}(s)\sum_{k=K+1}^{\infty}\Psi_k(s). \tag{3.13}$$

The equation of motion for the reduced density operator can be derived by evaluating the time derivative of the left- and right- hand-side wave functions and the influence functional. [70, 72, 66, 71, 73, 74] We consider the auxiliary matrix defined by

$$\begin{aligned}
\rho^{(n,m)}_{j_1,j_2,\ldots,j_K}(\bar{\psi},\psi';t) =& \int D[\bar{\psi}(\tau)]D[\psi(\tau)]D[\bar{\psi}'(\tau)]D[\psi'(\tau)]\\
&\times\mathrm{e}^{iS_A[\bar{\psi},\psi]/\hbar}F^{(n,m)}_{j_1,\cdots,j_K}[\bar{\psi},\psi,\bar{\psi}',\psi';t]\mathrm{e}^{-iS_A[\bar{\psi}',\psi']/\hbar},
\end{aligned} \tag{3.14}$$

where

$$F^{(n,m)}_{j_1,\cdots,j_K}[\bar{\psi},\psi,\bar{\psi}',\psi';t] = \left\{\int_{t_0}^{t} du\Theta_-(u)\mathrm{e}^{-\left(\frac{\gamma}{2}-i\zeta\right)(t-u)}\right\}^n$$
$$\times\left\{\int_{t_0}^{t} du\Theta_+(u)\mathrm{e}^{-\left(\frac{\gamma}{2}+i\zeta\right)(t-u)}\right\}^m$$
$$\times\prod_{k=1}^{K}\left\{\int_{t_0}^{t} du\Psi_k(u)\mathrm{e}^{-\nu_k(t-u)}\right\}^{j_k} F[\bar{\psi},\psi,\bar{\psi}',\psi';t]. \tag{3.15}$$

The reduced density matrix element at $t$ is represented as $\rho^{(n,m)}_{j_1,j_2,\cdots,j_K}(\bar{\psi}_f,\psi'_f;t)$ and then that at $t+\epsilon$ is obtained in the path integral form by inserting the completeness relation into the reduced density matrix at $t$ by

$$\rho^{(n,m)}_{j_1,\cdots,j_K}(\bar{\psi}_f,\psi'_f;t+\epsilon) = \mathrm{T}\left(\int d\bar{\psi}d\psi d\bar{\psi}'d\psi'\right.$$
$$\times\mathrm{e}^{-\bar{\phi}_1\bar{\phi}_2\phi_1\phi_2-\bar{\phi}_2\phi_2}$$
$$\times\langle\psi_f|\mathrm{e}^{-\frac{i}{\hbar}\hat{H}_A\epsilon}|\psi\rangle\langle\psi|\mathrm{e}^{-\frac{i}{\hbar}\hat{H}_A(t-t_0)}|\psi_0\rangle$$
$$\times F^{(n,m)}_{j_1,j_2,\cdots,j_K}(t+\epsilon)\langle\psi'_0|\mathrm{e}^{\frac{i}{\hbar}\hat{H}_A(t-t_0)}|\psi'\rangle\langle\psi'|\mathrm{e}^{\frac{i}{\hbar}\hat{H}_A\epsilon}|\psi'_f\rangle.$$
$$\left.\times\ \mathrm{e}^{-\bar{\phi}'_1\bar{\phi}'_2\phi'_1\phi'_2-\bar{\phi}'_2\phi'_2}\right). \tag{3.16}$$

We expand both sides of Eq. (3.16) with respect to $\epsilon$ and integrate the right side with respect to Grassmann numbers $\bar{\psi}$, $\psi$, $\bar{\psi}'$, and $\psi'$ following the Berezin's rule.[79]

Then by taking the limit $\epsilon$ to 0, we have

$$\begin{aligned}
&\frac{\partial}{\partial t}\rho^{(n,m)}_{j_1,\cdots,j_K}(\bar{\psi}_f,\psi'_f) = \int d\bar{\psi}d\psi d\bar{\psi}'d\psi' \\
&\times\Bigg\{-\left[\frac{i}{\hbar}\left(H_A(\bar{\psi}_f,\psi)-H_A(\bar{\psi}',\psi'_f)\right)+\frac{(n+m)\gamma}{2}\right. \\
&\left.-i(n-m)\zeta+\sum_{k=1}^{K}j_k\nu_k-\hat{\Xi}\right]\rho^{(n,m)}_{j_1,\cdots,j_K}(\bar{\psi},\psi';t) \\
&+V^{\times}\rho^{(n+1,m)}_{j_1,\cdots,j_K}(\bar{\psi},\psi';t)+n\Theta_-\rho^{(n-1,m)}_{j_1,\cdots,j_K}(\bar{\psi},\psi';t) \\
&+V^{\times}\rho^{(n,m+1)}_{j_1,\cdots,j_K}(\bar{\psi},\psi';t)+m\Theta_+\rho^{(n,m-1)}_{j_1,\cdots,j_K}(\bar{\psi},\psi';t) \\
&+\sum_{k=1}^{K}V^{\times}\rho^{(n,m)}_{j_1,\cdots,j_k+1,\cdots,j_K}(\bar{\psi},\psi';t) \\
&+\sum_{k=1}^{K}j_k\nu_k\Psi_k\rho^{(n,m)}_{j_1,\cdots,j_k-1,\cdots,j_K}(\bar{\psi},\psi';t)\Bigg\}, \qquad (3.17)
\end{aligned}$$

where $V^{\times}\equiv V(\bar{\psi}_f,\psi)-V(\bar{\psi}',\psi'_f)$ and $V^{\circ}\equiv V(\bar{\psi}_f,\psi)+V(\bar{\psi}',\psi'_f)$. $\Theta_{\pm}$, $\Psi_k$, and $\Xi$ are obtained by replacing $\hat{V}^{\times}\rightarrow V^{\times}$ and $\hat{V}^{\circ}\rightarrow V^{\circ}$ in equations (3.9)-(3.13) . The equation (3.17) is converted to the hierarchy equations of motion in operator form as

$$\begin{aligned}
\frac{d}{dt}\hat{\rho}^{(n,m)}_{j_1,\cdots,j_K}(t) \quad &= -\hat{\mathcal{L}}^{(n,m)}\hat{\rho}^{(n,m)}_{j_1,\cdots,j_K}(t) \\
&+\hat{V}^{\times}\hat{\rho}^{(n+1,m)}_{j_1,\cdots,j_K}(t)+n\hat{\Theta}_-\hat{\rho}^{(n-1,m)}_{j_1,\cdots,j_K}(t) \\
&+\hat{V}^{\times}\hat{\rho}^{(n,m+1)}_{j_1,\cdots,j_K}(t)+m\hat{\Theta}_+\hat{\rho}^{(n,m-1)}_{j_1,\cdots,j_K}(t) \\
&+\sum_{k=1}^{K}\hat{V}^{\times}\hat{\rho}^{(n,m)}_{j_1,\cdots,j_k+1,\cdots,j_K}(t) \\
&+\sum_{k=1}^{K}j_k\nu_k\hat{\Psi}_k\hat{\rho}^{(n,m)}_{j_1,\cdots,j_k-1,\cdots,j_K}(t), \qquad (3.18)
\end{aligned}$$

where

$$\hat{\mathcal{L}}^{(n,m)} = \frac{i}{\hbar}\hat{H}_A^{\times} + \frac{(n+m)\gamma}{2} - i(n-m)\zeta + \sum_{k=1}^{K} j_k\nu_k - \hat{\Xi} \tag{3.19}$$

and $\hat{\Theta}_{\pm}$, $\hat{\Psi}_k$, and $\hat{\Xi}$ are the operator forms of Eqs. (3.9), (3.10), and (3.13) which are obtained by replacing $V^{\times}(t)\rho$ with $\hat{V}\hat{\rho}(t) - \hat{\rho}(t)\hat{V}$ and $V^{\circ}(t)\rho(t)$ with $\hat{V}\hat{\rho}(t) + \hat{\rho}(t)\hat{V}$.

As can be seen from the form of equations, the $(n, m, j_1, \cdots, j_K)$th member of the hierarchy is coupled to the lower- and higher-order members as $\hat{\rho}^{(n\pm1,m)}_{j_1,\cdots,j_K}$, $\hat{\rho}^{(n,m\pm1)}_{j_1,\cdots,j_K}$, $\hat{\rho}^{(n,m)}_{j_1\pm1,\cdots,j_K}$, etc. In this approach, the 0th member of the hierarchy is the exact solution of the total Hamiltonian Eq. (2.3) defined by $\hat{\rho}^{(0,0)}_{0,\cdots,0}(t) = tr_{x'_\alpha}\{\hat{\rho}_{tot}(t)\}$ and it includes all orders of the system-bath interactions. Then the orders of system-bath interactions in $\hat{\rho}^{(n,m)}_{j_1,\cdots,j_K}(t)$ are lower than that in $\hat{\rho}^{(0,0)}_{0,\cdots,0}(t)$ by $N$ ($N \equiv n + m + \sum_k j_k$), since we defined the time derivative of $F$ in Eq. (3.15) by excluding the factor $(V^{\times})^N$. Thus, the present approach conceptually differs from the conventional perturbative expansion approaches; in such approaches, the 0th member includes no system-bath interactions and thus higher members take into account higher-order system-bath interactions.[66] Because of this hierarchical structure, we can handle strong system-bath interactions and non-white-noise baths.

To truncate the infinite hierarchy, we formally solve the eq. (3.18):

$$\rho^{(n,m)}_{j_1,\cdots,j_K} = \int_{t_0}^{t} d\tau \mathrm{e}^{\mathcal{L}(t-\tau)} g(\tau), \tag{3.20}$$

where

$$\mathcal{L} = -\left[\frac{i}{\hbar}\hat{H}_A^{\times} + \frac{(n+m)\gamma}{2} - i(n-m)\zeta + \sum_{k=1}^{K} j_k\nu_k - \hat{\Xi}\right] \tag{3.21}$$

and

$$
\begin{aligned}
g(\tau) &= \hat{V}^{\times}\hat{\rho}^{(n+1,m)}_{j_1,\cdots,j_K}(\tau) + n\hat{\Theta}_{-}\hat{\rho}^{(n-1,m)}_{j_1,\cdots,j_K}(\tau) \\
&\quad + \hat{V}^{\times}\hat{\rho}^{(n,m+1)}_{j_1,\cdots,j_K}(\tau) + m\hat{\Theta}_{+}\hat{\rho}^{(n,m-1)}_{j_1,\cdots,j_K}(\tau) \\
&\quad + \sum_{k=1}^{K}\hat{V}^{\times}\hat{\rho}^{(n,m)}_{j_1,\cdots,j_k+1,\cdots,j_K}(\tau) \\
&\quad + \sum_{k=1}^{K} j_k\nu_k\hat{\Psi}_k\hat{\rho}^{(n,m)}_{j_1,\cdots,j_k-1,\cdots,j_K}(\tau). \qquad (3.22)
\end{aligned}
$$

If the condition

$$
n + m + \sum_{k=1}^{K} j_k = N_{max} \gg \frac{\max\{\Omega_l - \Omega_m\}_{l,m}}{\min\left(\frac{\gamma}{2}, \nu_1\right)}, \qquad (3.23)
$$

is satisfied, $\frac{(n+m)\gamma}{2} + \sum_{k=1}^{K} j_k\nu_k$ is much larger than the characteristic time of the main system $\{\Omega_l - \Omega_m\}_{lm}$ because $\Gamma^{(n,m)} \geq N_{max}\min\left(\frac{\gamma}{2}, \nu_1\right)$. Then Eq. (3.21) is approximated as

$$
\Gamma^{(n,m)}\mathrm{e}^{\Gamma^{(n,m)}(t-\tau)} \simeq \delta(t-\tau), \qquad (3.24)
$$

which leads Eq. (3.18) to the terminator

$$
\frac{d}{dt}\hat{\rho}^{(n,m)}_{j_1,\cdots,j_K}(t) = -\left[\frac{i}{\hbar}\hat{H}^{\times}_{A} - i(n-m)\zeta - \hat{\Xi}\right]\hat{\rho}^{(n,m)}_{j_1,\cdots,j_K}(t). \qquad (3.25)
$$

# Chapter 4

# Time-evolution of the Density Matrix Elements

We fix the frequency of the oscillators in the ($P$, $Q$) space as $\omega_0 = 500\text{cm}^{-1}$ ($1/\omega_0$=66.7fs) and used it as the unit of the system. The vibrational motion along the reaction coordinate is in quantum regime at room temperature, since we have $\beta\hbar\omega_0 = 2.40$ for the temperature $T = 300\text{K}$.

Throughout this paper, we also fix the energies of $|3\rangle$ as $\Omega_3 = 0$, the nonadiabatic coupling between $|1\rangle$ and $|3\rangle$ as $\Delta_{13} = \Delta_{31} = 0$ and the individual coupling constants between the electronic state and the oscillator mode as $d_1 = -0.5$, $d_2 = 0$, and $d_3 = 0.5$. The displacement of the ($P$, $Q$) oscillators $\lambda$, the coupling strength between the oscillators and the bath $\gamma$, the temperature $T$, the energy of the initial and the intermediate state $\Omega_1$ and $\Omega_2$ are then changed independently to study the parameter dependence on the time evolution of the density matrix and the ET reaction rate.

In the chapters 3 and 4 we set $\Omega_2 = -\omega_0$, $\Delta_{12} = \Delta_{21} = 0.1\omega_0$ and $\Delta_{23} = \Delta_{32} = 0.1\omega_0$ unless otherwise noted.

To calculate the time-evolution of the density matrix elements, we set the initial populations as $\rho_1(0) = 1$ and $\rho_2(0) = \rho_3(0) = 0$, where $\rho_j(t)$ represents the population of the $|j\rangle$ state at time $t$. Experimentally such initial condition can be prepared by applying a short laser pulse to instantaneously excite the $|1\rangle$ state from other outside states (neither $|2\rangle$ nor $|3\rangle$).

Hierarchy equations of motion for the reduced density matrix Eqs. (3.18) and (3.25) are then solved via the fourth-order Runge-Kutta method, in which the time step is $0.01/\omega_0$. We chose the depth of the hierarchy and the truncation number of the hierarchy $K = 5$ and $N = 15$ for a low temperature case ($T = 10$K), $K = 3$ and $N = 15$ for intermediate temperature cases ($120\text{K} \leq T \leq 600\text{K}$), $K = 2$ and $N = 15$ for $T = 900$K, and $K = 1$ and $N = 15$ for high temperature cases ($T \geq 1500$K), respectively. For all calculations, the accuracies were checked by changing the values of $K$ and $N$.

## 4.1 Effects of the displacement $\lambda$

Figures 4.1(a)-(e) show the time-evolution of the density matrix elements for various displacements of the ($P$, $Q$) oscillators represented by $\lambda$. Here, we chose $\gamma = 0.1\omega_0$ and $T = 300$K. Fig. 4.1 (a) illustrates the case that the displacements between the oscillators are zero ($\lambda = 0$). In this case, the profiles of wavepackets in each ($P$, $Q$) potentials in the $|1\rangle$, $|2\rangle$, and $|3\rangle$ states do not change via the nonadiabatic transitions due to their optical Condon transition like character. [27, 28, 29] Since the heat-bath can affect the system only through the ($P$, $Q$) space wavepacket dynamics and the

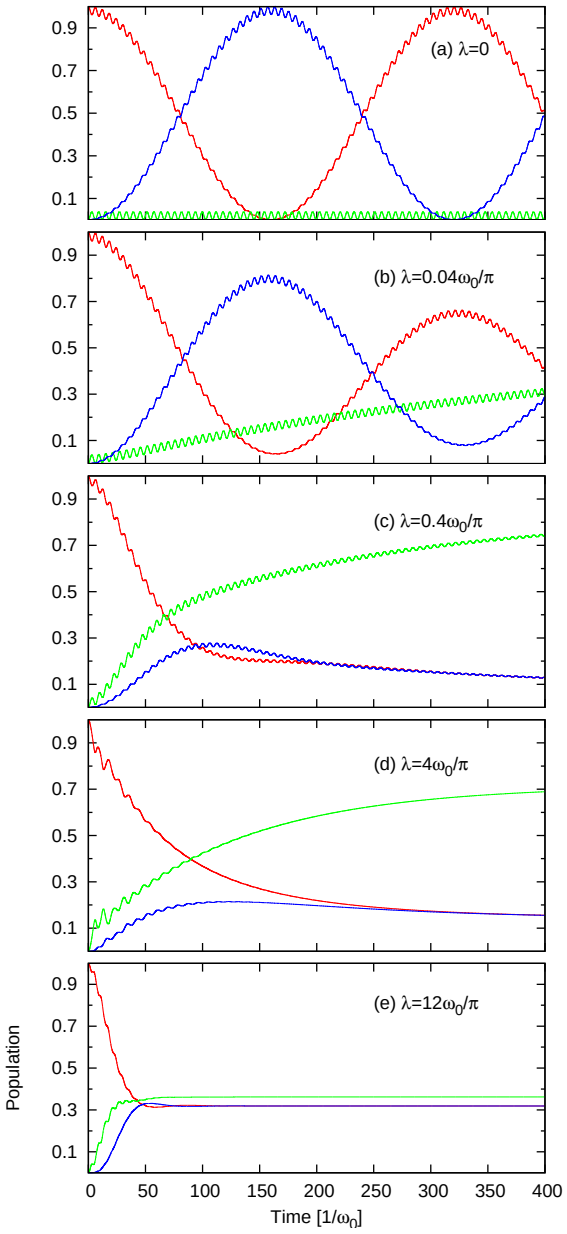


Figure 4.1: Time-evolution of the density matrix elements for the different displacement of (P, Q) oscillators $\lambda$ =(a) 0, (b) $0.04\omega_0/\pi$, (c) $0.4\omega_0/\pi$, (d) $4\omega_0/\pi$, and (e) $12\omega_0/\pi$. We chose $\gamma = 0.1\omega_0$, $\Omega_2 = -\omega_0$, and $T = 300$K. In each figures, the red, green, and blue lines show $\rho_1(t)$, $\rho_2(t)$, and $\rho_3(t)$, respectively. We employ (d) $\lambda = 4\omega_0/\pi$ as the reference in 4.2-5.

wavepackets are already in the equilibrium profiles with the temperature $T$, the heat-bath does not play any role if the displacement $D$ is zero. Thus, the time-evolution of $\rho_j(t)$, which reflects not the profile but the population of the $j$th wavepackets, exhibits only coherent motions between the three states. The frequencies of coherent motion can be analyzed by diagonalizing the three-state Hamiltonian described by $\Omega_j$ and $\Delta_{jk}$. Then the time evolution $\rho_1(t)$ is, for example, characterized by three frequencies $\Omega_R = 1.04\omega_0$, $\epsilon_-/\hbar = 1.02\omega_0$ and $\epsilon_+/\hbar = 0.0196\omega_0$, corresponding to the three transition frequencies between eigenstates (see Appendix B). This feature is peculiar to the multi-state system in contrast to the two-state case, where the motion is characterized by the Rabi frequency in NMR.

As $\lambda$ increases, the energy exchange between the $|j\rangle$ states and the bath becomes efficient and the low frequency part of the coherent motion is suppressed as illustrated Figs. 4.1 (b) and (c). The population of $|1\rangle$ undergoes the transition to $|3\rangle$ and eventually decays exponentially as illustrated in Fig. 4.1 (d). If the $\lambda$ becomes even larger, $\rho_j(t)$ quickly reaches to its equilibrium value as can be seen in Fig. 4.1 (e). If we regard the canonically transformed ($P$, $Q$) oscillator plus bath system as the bath for the three-state system, the conditions in Figs. 4.1 (d) and (e) are in the strong system-bath coupling regime which could not be handled by other reduced equation of motion approaches. If we adopt this picture, the coupling to the transformed bath causes frequency modulations of $|j\rangle$ and thereby shifts the eigen energies of $|1\rangle$ and $|3\rangle$ states to $\Omega_1' = \Omega_1 - \lambda/4$ and $\Omega_3' = \Omega_3 - \lambda/4$, respectively. Thus, while the equilibrium populations $\rho_2^{eq}$ decrease, those of $\rho_1^{eq}$ and $\rho_3^{eq}$ increase

for large $\lambda$ as illustrated in Figs. 4.1 (c)-(d).

## 4.2 Effects of the oscillator-bath coupling strength $\gamma$

The parameter $\gamma$ represents the coupling strength between the ($P$, $Q$) mode and the bath. It reflects the time-evolution of $\rho_j(t)$ through $J'(\omega)$ defined by Eq. (2.5). In Fig. 4.2, we display $\rho_j(t)$ for different $\gamma$ for fixed $\lambda = 4\omega_0/\pi$. The other parameters are the same as in Fig. 4.1. Fig. 4.2 (a) $\gamma = 0.01\omega_0$ is an underdamped case, whereas (c) $\gamma = \omega_0$ is an overdamped case for the ($P$, $Q$) space wavepacket motion.

In this model the ($P$,$Q$) oscillator becomes a part of the bath, so that the relaxation of this oscillator to thermal equilibrium must be much faster than the electron transfer process. This means that for small $\gamma$ the ET reaction rate must be much smaller than $\gamma$.[67] We have checked that the choice of $\gamma$ in the present study satisfies this criteria.

When $\gamma$ increases, the oscillatory motions in the ($P$, $Q$) potentials are suppressed as can be seen from Figs. 4.2 (a)-(c). Note that the effective coupling strength between the three-level system and the canonically transformed bath is evaluated as $J'(\omega = \Omega)/\Omega$,[82] where $\Omega$ is a characteristic frequency of the three-state system. Thus, $\rho_j(t)$ reaches their equilibrium values faster when $\gamma$ becomes larger because $J'(\omega = \Omega)/\Omega$ becomes larger. The strength of the effective damping for fast components $\Omega_R$ and $\epsilon_-/\hbar$ is in the order of (b)>(a)>(c), whereas that for slow components $\epsilon_+/\hbar$ is (c)>(b)>(a), which results in the fact that the relaxation profiles of $\rho_j(t)$ are

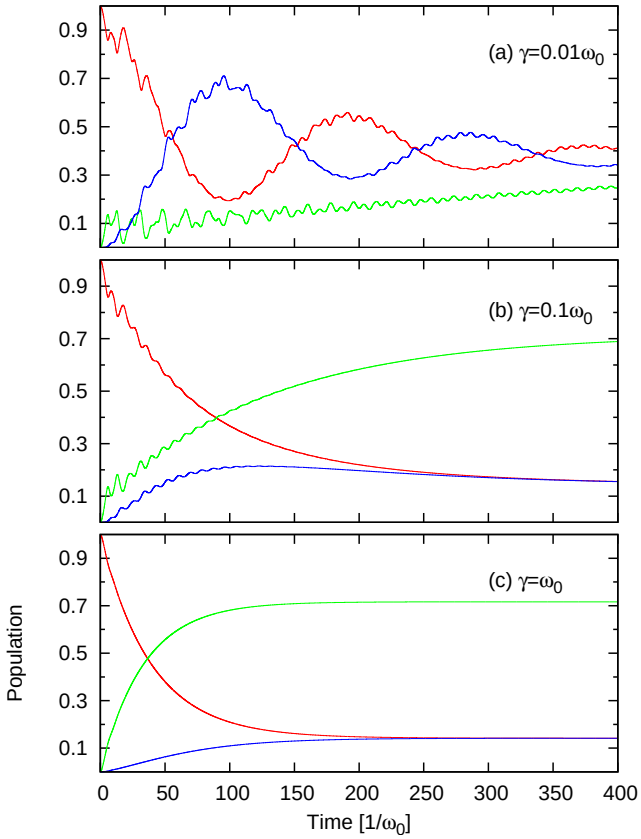


Figure 4.2: Time-evolution of the density matrix elements for different oscillator-bath coupling $\gamma$ =(a) $0.01\omega_0$, (b) $0.1\omega_0$, and (c) $\omega_0$. We set $\lambda = 4\omega_0/\pi$, so that the case (b) $0.1\omega_0$ agrees with Fig. 4.1 (d). The other parameters are the same as Fig. 4.1. In each figures, the red, green, and blue lines show $\rho_1(t)$, $\rho_2(t)$, and $\rho_3(t)$, respectively.

different even for the same $\lambda$.

## 4.3 Effects of the temperature $T$

Figures 4.3 (a)-(d) show the time evolution of $\rho_j(t)$ for various temperatures $T$. In these figures, the displacement is chosen to give $\lambda = 4\omega_0/\pi$. The other parameters are the same as those in Fig. 4.1. When $T$ goes down, the population of the $|2\rangle$ state increases since the energy of this state is the lowest in the present oscillators configuration. At any temperature fast oscillations are the result of ($P$, $Q$) motion. When $T$ goes down, the low-frequency oscillation originating from the transition between the electronic states becomes prominent. This is because the excited state motion of the ($P$, $Q$) mode, which can smear the electronic transition energies, is suppressed at temperatures below $T = 150$K. While $\rho_1$ decays exponentially at high temperature, it does not at $T = 10$K, since the dissipative ($P$, $Q$) oscillator mode plays a minor role.

## 4.4 Effects of the intermediate state energy $\Omega_2$

We now change the intermediate state energy $\Omega_2$, which is important to understand a role of activation energy in the ET process. Since we deal with a colored noise, the effective coupling strength $J'(\omega = \Omega)/\Omega$,[82] where $\Omega$ is a characteristic frequency, changes if $\Omega_j$ and $\Delta_{jk}$ change. To see the pure effects from the configuration, we compare the results with $\Omega_2 = \pm\omega_0$ and $\Omega_2 = \pm 10\omega_0$, which are illustrated in Figs. 4.4 and 4.5. While time-evolution

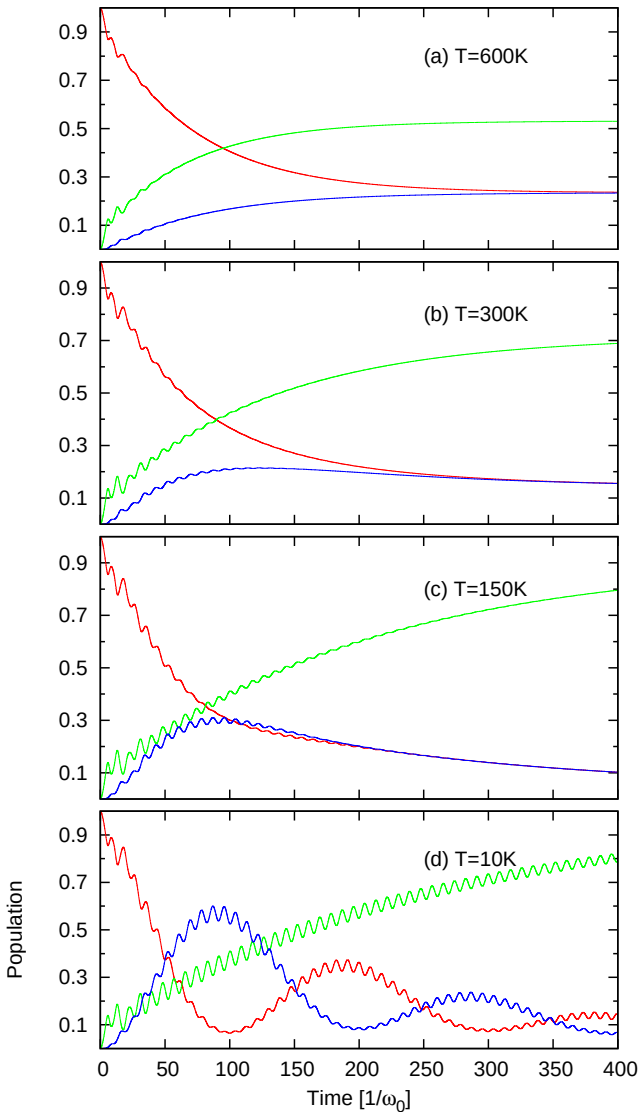


Figure 4.3: Time-evolution of the density matrix elements for different temperature $T$ =(a) 600K, (b) 300K, (c) 150K, and (d) 10K. We set $\lambda = 4\omega_0$, so that the other parameters are the same as Fig. 4.1. In each figures, the red, green, and blue lines show $\rho_1(t)$, $\rho_2(t)$, and $\rho_3(t)$, respectively.

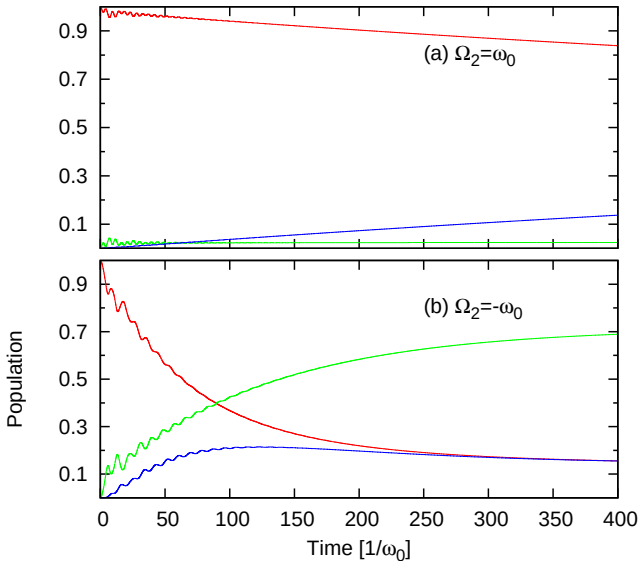


Figure 4.4: Time-evolution of the density matrix elements for (a) $\Omega_2 = \omega_0$ and (b) $\Omega_2 = -\omega_0$. We set $\lambda = 4\omega_0/\pi$, $\gamma = 0.1\omega_0$ and $T = 300$K so that the case (b) $\Omega_2 = -\omega_0$ agrees with Fig. 4.1 (d). In each figures, the red, green, and blue lines show $\rho_1(t)$, $\rho_2(t)$, and $\rho_3(t)$, respectively.

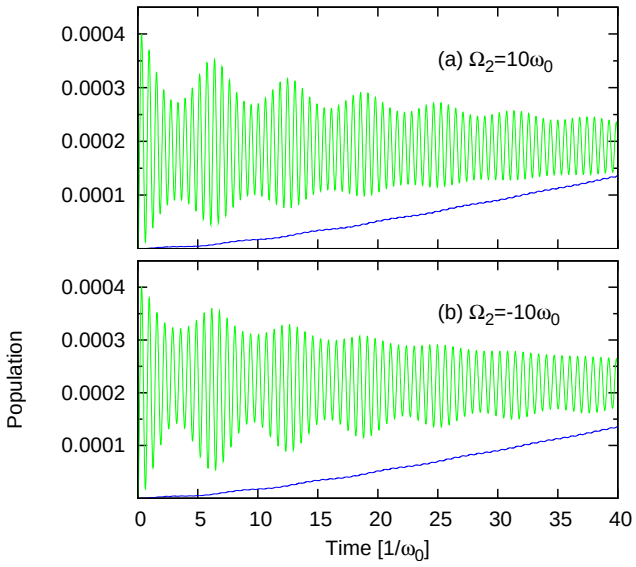


Figure 4.5: Same as Fig. 4.4 besides (a) $\Omega_2 = 10\omega_0$ and (b) $\Omega_2 = -10\omega_0$.

profiles for plus and minus results are similar for large $|\Omega_2|$, they are very different for small $|\Omega_2|$. This is due to the energy shifts of the electronic states arising from the interaction between the system and the canonically transformed bath. The system-bath interaction $-\hat{V}\sum c'_\alpha x'_\alpha$ induces energy fluctuations, which shift the energies of $|1\rangle$ and $|3\rangle$ states to $\Omega'_1 = \Omega_1 - \lambda/4$ and $\Omega'_3 = \Omega_3 - \lambda/4$. Since the effective damping strength is determined by $|\Omega_2 - \Omega'_1|$ and $|\Omega_2 - \Omega'_3|$, the difference of damping for positive and negative $|\Omega_2|$ becomes large for small $\Omega_2$. Thus, while the results in Fig. 4.4 (a) and Fig. 4.4 (b) are very different, those in Fig. 4.5 (a) and Fig. 4.5 (b) are similar.

## 4.5 Effects of the nonadiabatic coupling $\Delta_{jk}$

Finally we discuss the effects of the nonadiabatic couplings $\Delta_{12}$ and $\Delta_{23}$, which control the ET reaction in direct manner. Figures 4.6 (a)-(c) display the time-evolution of $\rho_j(t)$ for different nonadiabatic coupling strengths $\Delta_{12}$ and $\Delta_{23}$. For weak nonadiabatic coupling, as shown in Fig. 4.6 (a), the populations decay slowly. This result is in the nonadiabatic regime and the ET can be treated as the perturbation of the nonadiabatic coupling. The lowest order transition from $|1\rangle$ to $|3\rangle$ is second-order in both $\Delta_{12}$ and $\Delta_{23}$ and proportional to $\Delta_{12}^2\Delta_{23}^2$ (see Appendix B). When the nonadiabatic coupling becomes strong, higher-order contributions corresponding to the recrossing processes play a role. This is the diabatic transition regime where the diabatic representation of the potentials is applied to understand system dynamics (see, for example, Fig.2 in Ref. [20]). The populations exhibit oscillating features in the large nonadiabatic coupling case until about $t = 50$. In the classical picture, this phenomenon is explained by recrossing of the wavepacket between the potentials that failed to get trapped by dissipation process, but in the quantum picture, it is an interference phenomenon explained by the transition between the energy eigenstates.[20]

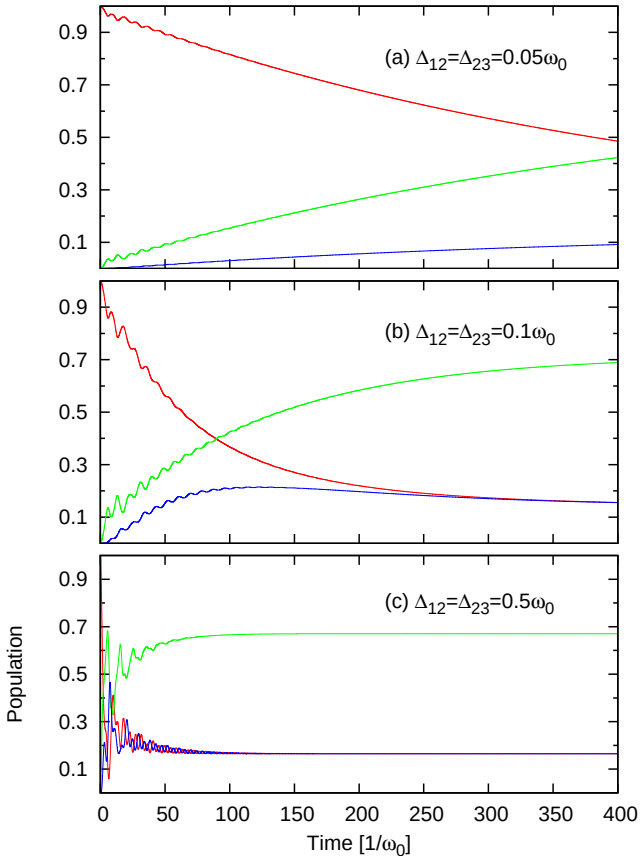


Figure 4.6: Time-evolution of the density matrix elements for different nonadiabatic couplings $\Delta_{12} = \Delta_{23} =$ (a) $0.05\omega_0$, (b) $0.1\omega_0$, and (c) $0.5\omega_0$. We set $\lambda = 4\omega_0/\pi$, $\gamma = 0.1\omega_0$ and $T = 300$K. The case (b) $\Delta_{12} = \Delta_{23} = 0.1\omega_0$ agree with Fig. 4.1 (d). In each figures, the red, green, and blue lines show $\rho_1(t)$, $\rho_2(t)$, and $\rho_3(t)$, respectively.

# Chapter 5

# Electron Transfer Reaction Rate

As shown in IV, $\rho_j(t)$ decays more or less exponentially apart from the initial temporal oscillatory motions. Since the chemical reaction rate can be defined by the flux-flux correlation function, which is the correlation function between the population of reactant and product states, the present ET reaction process may also be characterized by $\rho_j(t)$. Because the difference from the equilibrium population $\delta\rho(t) = \rho(t) - \rho^{eq}$ is expected to approach zero with time as $\delta\rho(t) = \delta\rho(0) \cdot \mathrm{e}^{-kt}$, the ET rate can be defined in a time-dependent form[83]

$$k(t) = -\frac{\dot{\delta\rho}(t)}{\delta\rho(t)}. \tag{5.1}$$

In order to obtain the rate in the three-state ET reaction, we computationally perform linear response experiments.[72, 82] First, we set the energy of the $|3\rangle$ state to $\Omega_3 + \epsilon$, where $\epsilon$ is small ($0.01\omega_0$) and the populations of electronic states to their thermodynamic averages. After a sufficient time, for which the system reaches equilibrium, we set the present time as $t = 0$

and remove the perturbation $\epsilon$. The populations at $t = 0$, equilibrated with the perturbation, are no longer in equilibrium and re-equilibrate to the unperturbed state. Then, we adapt the definition of the time-dependent ET rate, Eq. (5.1), for the three-state system as $k(t) = -\dot{\delta\rho_3}(t)/\delta\rho_3(t)$. Since $\delta\rho_3(t)$ and $\dot{\delta\rho_3}(t)$ are expected to be proportional to the perturbation $\epsilon$ if $\epsilon$ is small, $k(t)$ does not depend on $\epsilon$.

To illustrate the feature of ET rates, we plot the ET reaction rate as a function of time for different $\gamma$ in Fig. 5.1. The other parameters are the same as the case in Fig. 4.2. For weak $\gamma$, ET rates show an oscillation feature, because of the interference of transition between the discrete energy states at different potentials.[82] In a classical picture, the oscillation feature is interpreted as the recrossing of the population between the potentials caused by the electron that is not trapped. [20] After the temporal motions ends owing to the dissipation arising from the bath, the ET rate reaches plateau values. These plateau values, hereafter denoted by $k_{rxn}$, correspond to the relaxation rates. In the following, we ploted $k_{rxn}$ as the function of $T$, $\Omega_2$, and $\Omega_1$ to characterize the ET processes.

## 5.1 ET rate as the function of the inverse temperature

Figure 5.2 displays $k_{rxn}$ as the function of the inverse temperature $\beta\hbar\omega_0$. To analyze the temperature dependence of $k_{rxn}$, it is helpful to adopt the diabatic picture of the ET processes. The activation energies in this picture are estimated from the difference between the potential minima and the

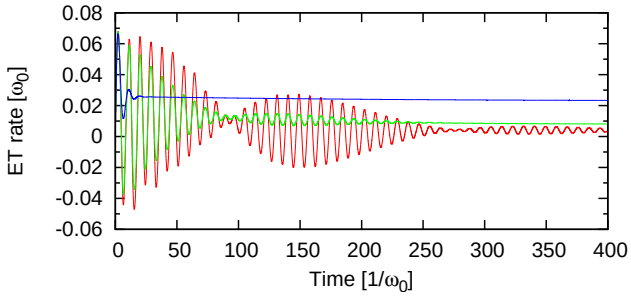


Figure 5.1: ET reaction rates for $\gamma = 0.05\omega_0$ (red line), $0.1\omega_0$ (green line), and $\omega_0$ (blue line). The other parameters are the same as Fig. 4.2

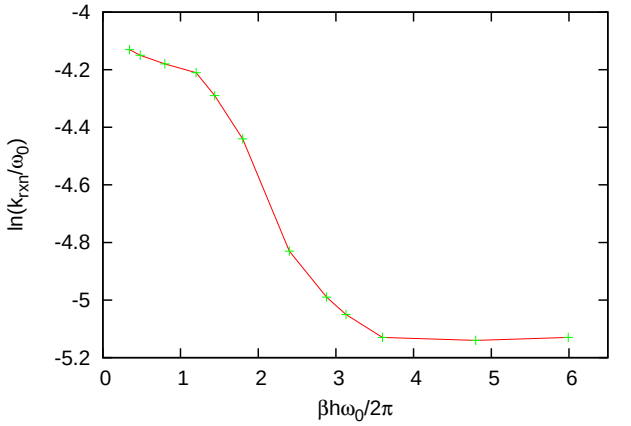


Figure 5.2: The relaxation rate as a function of the inverse temperature.

crossing points of the potentials. The activation energies between $|1\rangle$ and $|2\rangle$ and $|2\rangle$ and $|3\rangle$ are then evaluated as $E_{12}^{\neq} = 0.104\hbar\omega_0$ and $E_{23}^{\neq} = 0.785\hbar\omega_0$, respectively. Since we defined the ET rate by Eq. (5.1), the reactant state involves both the $|1\rangle$ and $|2\rangle$ states. When the temperature is high ($\beta\hbar\omega_0 < 1$), both $|1\rangle$ and $|2\rangle$ states are populated and both $|1\rangle \rightarrow |2\rangle \rightarrow |3\rangle$ and $|2\rangle \rightarrow |3\rangle$ transitions contribute to the ET rate. Since the $|1\rangle$ to $|3\rangle$ transition is harder than $|2\rangle$ to $|3\rangle$ and population in the $|1\rangle$ state cannot be negligible for $\beta\hbar\omega_0 < 1$, the gradient of the ET rate as a function of $\beta\hbar\omega_0$ becomes gentle in $\beta\hbar\omega_0 < 1$, The ET rates follows the Arrhenius law of the $|2\rangle \rightarrow |3\rangle$ transition with the activation energy $E_{23}^{\neq} = 0.785\hbar\omega_0$.

The ET process is an intrinsically quantum process and the reaction rate reflects not only energy gaps but also the overlap of wave functions. For low temperature $\beta\hbar\omega_0 > 3.60$, the wavepackets are localized at the ground state of $|2\rangle$. Since the profile of a wavepacket does not change much below this temperature, the ET rate, which can also be calculated from the overlap of integrals of $|2\rangle$ and $|3\rangle$ wavepackets, become constants.

## 5.2 ET rate as the function of $\Omega_2$ and $\Omega_1$

Figures 5.3 and 5.4 illustrate the ET reaction rates as a function of $\Omega_2$ and $\Omega_1$ evaluated from the linear response simulation. The other parameters are the same as those in Fig. 4.1. In contrast to the results from the two-state system whose ET rate profile is characterized by so called "inverted parabola" (see also Appendix C),[63, 84, 1, 51, 52, 53, 4] the ET rates in the three-state case exhibits an asymmetric bell shape as shown in Fig. 5.3. The

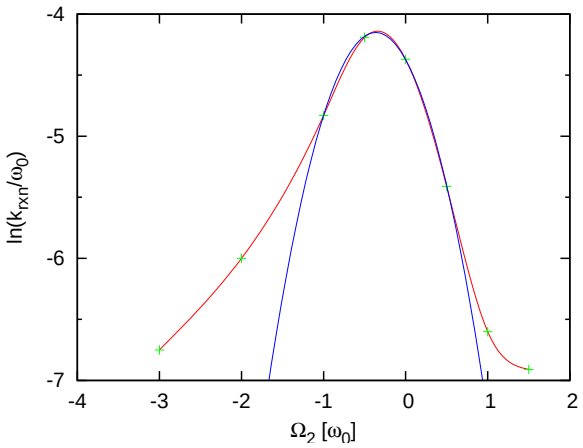


Figure 5.3: The relaxation rate as a function of $\Omega_2$. Resultant values of $\ln(k_{rxn}/\omega_0)$ (green points) are fitted to the spline function (red line), and those of $\Omega_2 = -\omega_0$, $-0.5\omega_0$, 0, and $0.5\omega_0$ are fitted to the parabola (blue line).

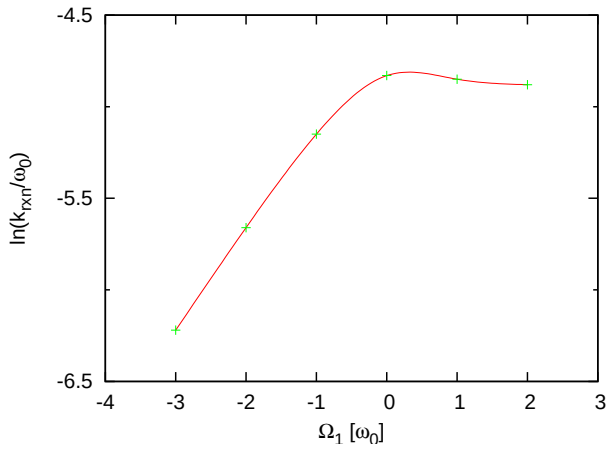


Figure 5.4: The relaxation rate as a function of $\Omega_1$. We set $\Omega_2 = -\omega_0$ and $\Omega_3 = 0$.

top of the parabola is not formed at $\Omega_2 = 0$ but at $\Omega_2 = -\lambda/4$, since the ($P$, $Q$) oscillator plus bath system shifts the energies of both the $|1\rangle$ and $|3\rangle$ states. For $\Omega_2 \gg \omega_0$, $\ln k_{rxn}$ does not decrease so much, since the quantal super-exchange transition mechanism plays a major role in this parameter regime.[32, 33] This process arises from the coherent transition between $|1\rangle$ and $|3\rangle$, which utilizes the coherences between $|1\rangle$ and $|2\rangle$ and $|2\rangle$ and $|3\rangle$, and is similar to the second-order Raman process in the optical problem.[85, 86] Since the $|2\rangle$ state acts as the virtual state, the $\Omega_2$ dependence of the super-exchange transition is weaker than that of the thermally activated transition from $|1\rangle \rightarrow |2\rangle \rightarrow |3\rangle$. This transition is called a sequential transition and is analogous to the luminescence in optics. While the transition for $-\omega_0 < \Omega_2 < 0.5\omega_0$ is explained by the sequential transition which exhibits a normal inverted parabolic profile as a function of $\Omega_2$, $\ln(k_{rxn}/\omega_0)$ becomes larger than expected for $\Omega_2 < -\omega_0$. As explained before, both $|1\rangle$ and $|2\rangle$ states act as the reactant state by the definition $k(t)$ in Eq. (5.1). For small $\Omega_2$, the majority of the population is in the $|2\rangle$ state and the major contribution to the ET rate becomes the $|2\rangle \rightarrow |3\rangle$ transition, while the contribution from $|1\rangle \rightarrow |2\rangle \rightarrow |3\rangle$ transition becomes small due to the small $|1\rangle$ population. Since the transition rate of $|2\rangle \rightarrow |3\rangle$ is larger than that of $|1\rangle \rightarrow |2\rangle \rightarrow |3\rangle$ , the ET rate becomes larger than expected from the parabolic profile as indicated in Fig. 5.3.

Figure 5.4 displays the ET reaction rate as the function of $\Omega_1$ for fixed $\Omega_2 = -\omega_0$ and $\Omega_3 = 0$. For large $\Omega_1$, the majority of the population is in the $|2\rangle$ state and since only the $|2\rangle \rightarrow |3\rangle$ transition contributes to the ET rate,

the reaction rate becomes constant. For small $\Omega_1$, most population is in the $|1\rangle$ state. In this case the transition between $|2\rangle$ and $|3\rangle$ plays a minor role and the ET rate is mostly determined from the $|1\rangle \rightarrow |2\rangle$ transition. Then the profile of the ET rate exhibits an inverted parabolic shape for small $\Omega_1$ with the activation energy determined from the $|1\rangle$ and $|2\rangle$ states.

# Chapter 6

# Concluding Remarks

A kinetic equation of motion approach for reduced density matrix elements has an advantage to study dynamics in a large time scale, since such approach does not require the sampling which rapidly increases with an evolution time period and the degrees of freedom. While the majority of the reduced equation of motion approaches have to employ some approximations such as the rotating wave approximation, the white noise (or Van Hove) approximation, the factorized assumption for the system and the bath, all of which strongly restricts the applicability of the equations of motion. Such restrictions can be removed by introducing the hierarchy of reduced density matrices which contain the information of the higher-order system bath interactions.[66] Since many interesting problems including the ET processes are in the restricted parameter regimes of conventional reduced equations of motion approaches, the hierarchy equations of motion approach is variable especially to explore a nonlinear response, where the system-bath coherence neglected under factorization assumption plays a major role.

In this paper, we study the ET process by employing the hierarchy

equations of motion for the Brownian spectral distribution with the low-temperature correction terms.[19, 77] Taking an advantage of nonperturbative theory, we studied ET dynamics and ET reaction rates for the first time over a wide range of parameters including the system-bath coupling, nonadiabatic coupling and temperatures for various oscillators configurations. The time evolution of the reduced density matrix elements illustrates the interplay of coherences between the electronic and vibrational states. The ET reaction rates as a function of the intermediate state energy exhibits an asymmetric inverted parabolic profile in a small activation regime due to the presence of the intermediate state between the reactant and product states and a slowly decaying profile in a large activation energy regime, which arises from the quantum coherent transitions.

If necessary, further extension to a nonadiabatic transition problem with anharmonic potential surfaces[20, 21] with taking into account nonlinear oscillator-bath coupling[87, 88] is possible from the hierarchy equations of motion approach by explicitly dealing with the oscillator coordinate. Since we are dealing with equations of motion with the system-bath coherence, we can easily include the external time-dependent driving force to the system dynamics. Thus, nonlinear spectroscopy, such as multi-dimensional spectroscopy[89], is easily studied from the hierarchy equations of motion approach. Numerical rigorous solutions from this approach can provide information that can be compared with experimental results and approximate theory.

# Appendix A

# Derivation of the Brownian Spectral Density

As shown in Ref. [90], the reduced dynamics of just the electron and the single harmonic mode are influenced by the bath only through the following spectral density:

$$J_0(\omega) = \sum_\alpha \frac{c_\alpha^2}{2m_\alpha\omega_\alpha}\delta(\omega - \omega_\alpha). \tag{A.1}$$

The spectral density can be determined provided one knows the semiclassical equation of motion satisfied by the single harmonic mode. In particular, if, for fixed $\hat{V}$, the single harmonic mode experiences a frictional force linearly proportional to its velocity with a coefficient $M\gamma$, that is if the equation of motion is

$$M\frac{d^2Q}{dt^2} + M\gamma\frac{dQ}{dt} - M\omega_0^2 D\hat{V} = F_{ext}, \tag{A.2}$$

where $F_{ext}$ is any external force, then we can show that $J_0(\omega)$ is given by

$$J_0(\omega) = M\gamma\omega \exp\left[-\frac{\omega}{\omega_c}\right]. \tag{A.3}$$

Here, $\omega_c$ is a high frequency cutoff that is required on both physical and mathematical grounds, and that is much larger than the domain of frequencies over which Eq. (A.2) is a reasonable approximation to the exact equation of motion. (We taking the limit $\omega_c \to \infty$ later, so that (A.1) becomes $M\gamma\omega$ in 2.)

To determine the effective spectral density

$$J_{eff}(\omega) = \sum_\alpha \frac{c_\alpha'^2}{2m'_\alpha\omega'_\alpha}\delta(\omega - \omega'_\alpha), \tag{A.4}$$

we do not have to find $\{c'_\alpha\}$, $\{m'_\alpha\}$, etc. The transformation from Eq. (2.1) to Eq. (2.3) does not involve the electronic system, so that the same spectral density will control the dynamics of a continuous variable $q$ moving in some potential $U(q)$ and coupled to coordinates $Q$ and $\{x_\alpha\}$ in the same way as the electronic system. As shown by Leggett[91], it is enough to know the equation of motion for $q$ in the classical limit in order to deduce $J_{eff}(\omega)$, and this allows us to overcome the calculation of the normal modes.

For the purpose of finding $J_{eff}(\omega)$, we consider the Hamiltonian

$$\begin{aligned} H &= \frac{p^2}{2\mu} + U(q) + \frac{P^2}{2M} + \frac{1}{2}M\omega_0^2(Q - Dq)^2 \\ &\quad + \sum_\alpha \left\{ \frac{x_\alpha^2}{2m_\alpha} + \frac{1}{2}m_\alpha\omega_\alpha^2\left(x_\alpha - \frac{c_\alpha}{m_\alpha\omega_\alpha^2}Q\right)^2 \right\}, \end{aligned} \tag{A.5}$$

where $p$ is the momentum conjugate to $q$. The classical equations of motion are

$$\mu\ddot{q} = -\frac{dU(q)}{dq} + M\omega_0^2 D(Q - Dq), \tag{A.6}$$

$$M\ddot{Q} = -M\omega_0^2(Q - Dq) + \sum_\alpha c_\alpha x_\alpha - \sum_\alpha \frac{c_\alpha^2}{m_\alpha\omega_\alpha^2}Q, \tag{A.7}$$

and

$$m_\alpha \ddot{x}_\alpha^2 = -m_\alpha \omega_\alpha^2 x_\alpha + c_\alpha Q. \tag{A.8}$$

We define the Fourier transform

$$\tilde{q}(z) = \int_{-\infty}^{\infty} q(t) \mathrm{e}^{-izt} dt, \quad \mathrm{Im}(z) < 0, \tag{A.9}$$

and write the equation satisfied by $q$ as

$$\tilde{K}(z)\tilde{q}(z) = -\tilde{U}'(q), \tag{A.10}$$

where $\tilde{K}(z)$ is a function of $z$ alone, and $\tilde{U}'(q)$ is the Fourier transform of $dU(q)/dq$. Then, $J(\omega)$ is given by

$$J_{eff}(\omega) = \lim_{\epsilon \to 0+} \mathrm{Im}\left[\tilde{K}(\omega - i\epsilon)\right]; \ \omega \text{ real}. \tag{A.11}$$

Using the definitions (A.1) and (A.3), we obtain

$$\tilde{K}(z) = -\mu z^2 + M\omega_0^2 D^2 \frac{\tilde{L}(z)}{\tilde{L}(z) + M\omega_0^2}, \tag{A.12}$$

with

$$\tilde{L}(z) = -z^2 \left[ M + 2\int_0^\infty d\omega' \frac{M\gamma \mathrm{e}^{-\omega/\omega_c}}{\omega'^2 - z^2} \right]. \tag{A.13}$$

Here, we used the equation

$$\sum_\alpha \frac{c_\alpha^2}{m_\alpha \omega_\alpha^2 (\omega_\alpha^2 - z^2)} = 2\int_0^\infty d\omega' \frac{M\gamma \mathrm{e}^{-\omega'/\omega_c}}{\omega'^2 - z^2}. \tag{A.14}$$

After integrating the second term of the right side in (A.13), we take the cutoff $\omega_c$ to infinity, which then leads to the expression

$$\tilde{L}(z) = -z^2 M + iM\gamma z\pi. \tag{A.15}$$

Substituting this in Eq. (A.12), and using Eq. (A.11), we get

$$J_{eff}(\omega) = \frac{MD^2}{\pi} \frac{\gamma\omega\omega_0^4}{(\omega_0^2 - \omega^2)^2 + \omega^2\gamma^2}. \tag{A.16}$$

We introduce a parameter

$$\lambda \equiv \frac{M\omega_0^2 D^2}{2\hbar}, \tag{A.17}$$

then we get the Brownian spectral density (2.5).

# Appendix B

# Three-state Rabi Oscillation

To illustrate the characteristic motion arising from the three-state system, we analytically solve equation of motion for $\hat{H}_A$ defined by Eq. (2.2). We consider the probability that the system is initially ( at $t = 0$ ) in the state $|1\rangle$ and found in the state $|j\rangle$ at time $t$,

$$P_{j1}(t) \equiv |\langle j|U(t,0)|1\rangle|^2, \tag{B.1}$$

where $U(t,0)$ is the time evolution operator. To simplify the results, we assume $\Omega_1 = \Omega_3 = 0$, $\Delta_{12} = \Delta_{21}$, and $\Delta_{23} = \Delta_{32}$. Then the eigenvalues of $\hat{H}_A$ is given by $\epsilon = 0$ and $\epsilon_\pm \equiv \hbar(\Omega_2 \pm \Omega_R)/2$, where

$$\Omega_R = \sqrt{\Omega_2^2 + 4(\Delta_{12}^2 + \Delta_{23}^2)} \tag{B.2}$$

and the corresponding eigenstates are

$$|\chi_0\rangle = \frac{1}{\sqrt{\Delta_{12}^2 + \Delta_{23}^2}}(\Delta_{23}|1\rangle - \Delta_{12}|3\rangle), \tag{B.3}$$

and

$$|\chi_\pm\rangle = c_\pm \left(\Delta_{12}|1\rangle + \frac{\epsilon_\pm}{\hbar}|2\rangle + \Delta_{23}|3\rangle\right), \tag{B.4}$$

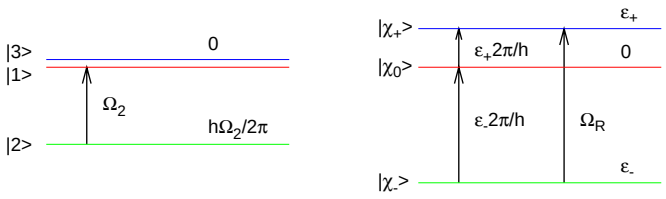


Figure B.1: Schematic view of the nondiagonal energies (left) and eigenenergies (right) of a three-state system. Beside the arrows are the characteristic frequencies of the system $\Omega_2$ (left), $\epsilon_\pm/\hbar$, and $\Omega_R$ (right).

where $c_\pm = (\Delta_{12}^2 + \Delta_{23}^2 + \epsilon_\pm^2/\hbar)^{-1/2}$ (see Fig. B.1.) The time evolution operator is thus expressed as

$$\begin{aligned} U(t,0) \quad &= |\chi_0\rangle\langle\chi_0| + |\chi_+\rangle e^{-\frac{i}{\hbar}\epsilon_+ t}\langle\chi_+| \\ &\quad +|\chi_-\rangle e^{-\frac{i}{\hbar}\epsilon_- t}\langle\chi_-|, \end{aligned} \tag{B.5}$$

in the $|1\rangle$, $|2\rangle$, and $|3\rangle$ basis sets. The probability of the system to be found in the state $|2\rangle$ and $|3\rangle$ at $t$ aregiven, respectively, by

$$P_{21}(t) = \frac{2\Delta_{12}^2}{\Omega_R^2}\sin^2\left(\frac{\Omega_R}{2}t\right), \tag{B.6}$$

and

$$\begin{aligned} P_{31}(t) = \quad & \frac{4\Delta_{12}^2\Delta_{23}^2}{\Delta_{12}^2+\Delta_{23}^2}\left\{c_+^2\sin^2\left(\frac{\epsilon_+}{2\hbar}t\right) + c_-^2\sin^2\left(\frac{\epsilon_-}{2\hbar}t\right)\right. \\ & \left. -\frac{1}{\Omega_R^2}\sin^2\left(\frac{\Omega_R}{2}t\right)\right\}. \end{aligned} \tag{B.7}$$

Thus the oscillation of $\rho_2(t)$ in the chapter 4 depends on $\Omega_R$, while those of $\rho_1(t)$ and $\rho_3(t)$ are determined by $\Omega_R$, $\epsilon_+/\hbar$, and $\epsilon_-/\hbar$.

# Appendix C

# Electron Transfer Rate in a Two-state Case

We can adapt the hierarchy equations of motion Eqs. (3.18) and (3.25) to the two-state case ($|1\rangle$ and $|2\rangle$) by simply truncating the sum of $j$ up to 2 in Eqs. (2.2) and (2.4), respectively. We set $\Omega_2 = 0$ and $\Delta_{12} = \Delta_{21} = 0.1\omega_0$ and employ the same bath parameters as in the section 5.2. The ET rate $k(t)$ is defined in terms of $\delta\rho_2(t)$ and the perturbation $\epsilon$ is put on $\Omega_2$ to carry out the linear response simulation. Figure C.1 shows the ET reaction rate as a function of activation energy. In this low friction regime, the ET reaction rate increases as energy mismatching is small.[92] The profile for the two-state system is parabolic as predicted by Marcus. In Fig. C.1, resultant values of $\ln(k_{rxn})$ are fitted to the parabola, $-0.168(x + 3.51 \times 10^{-11})^2 - 3.12$.

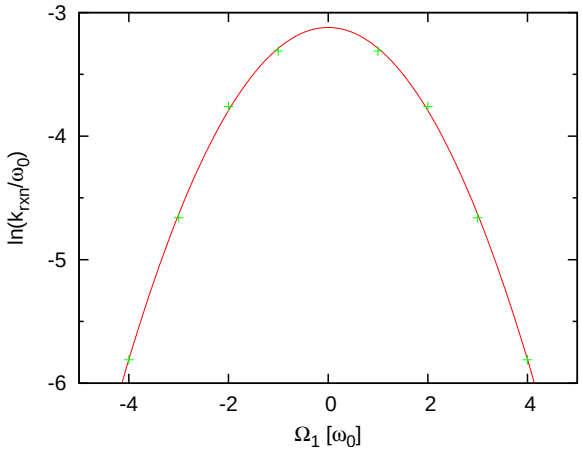


Figure C.1: The ET rate as a function of $\Omega_1$. Resultant values of $\ln(k_{rxn}/\omega_0)$ (green points) are fitted to the parabola. We set $\Omega_2 = 0$, and $\Delta_{12} = \Delta_{21} = 0.1\omega_0$, and $\lambda = 4\omega_0/\pi$. The other bath parameters are the same as in Fig. 4.2 (b)

# Appendix D

# Time-dependent Electron Transfer Rate

We illustrate ET rate as a function of time for different $\lambda$ in Fig. D.1, $T$ in Fig. D.2, and $\Omega_2$ in Fig. D.3. ET rates show an oscillation feature corresponding to the fine oscillation shown in Figs. 4.2, 4.3, and 4.4, which reflects the population transition between the discrete energy states. In Fig. D.1, the oscillation frequency is: $0.724\omega_0$ for $\lambda = 4\omega_0/\pi$; $0.388\omega_0$ for $\lambda = 8\omega_0/\pi$. In Fig. D.2, the oscillation of $k(t)$ has the same frequency $0.724\omega_0$ for all $T$ values. The above frequencies correspond to the fine oscillation of the population in the chapter 3.

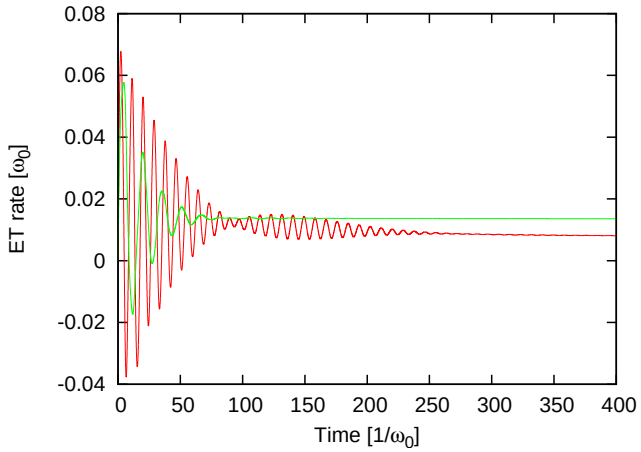


Figure D.1: ET reaction rates for $\lambda = 4\omega_0/\pi$ (red line) and $8\omega_0/\pi$ (green line). The other parameters are the same as Fig. 4.1.

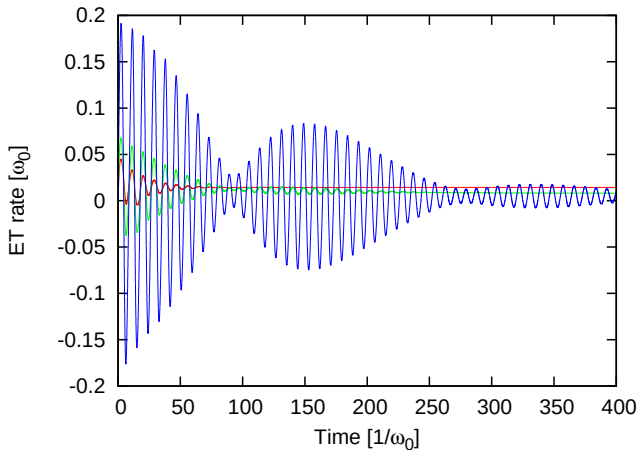


Figure D.2: ET reaction rates for $T = 600$K (red line), 300K (green line), and 150K. The other parameters are the same as Fig. 4.3.

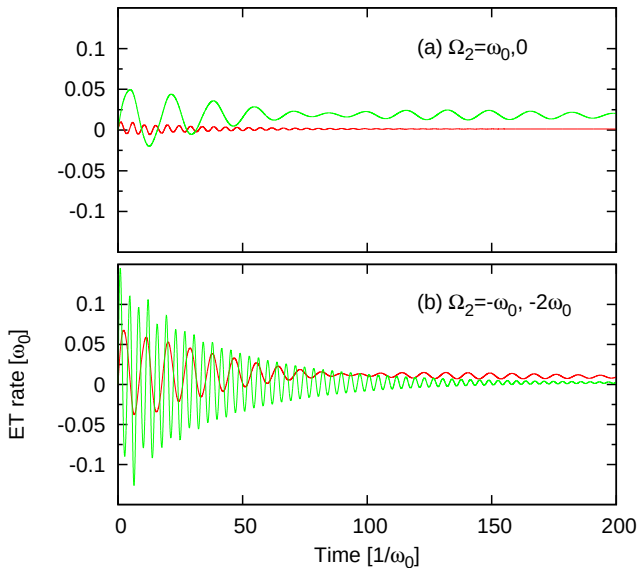


Figure D.3: ET reaction rates for different $\Omega_2$ values. Red and green lines show $k(t)/\omega_0$ in the case of $\Omega_2 = \omega_0$ and $\Omega_2 = 0$ in (a), and $\Omega_2 = -\omega_0$ and $\Omega_2 = -2\omega_0$ in (b).

# Bibliography


[1] R. A. Marcus, Rev. Mod. Phys. **65**, 599 (1993).

[2] V. May and O. Kühn, *Charge and Energy Transfer Dynamics in Molecular Systems* (Wiley-VCH, 2003).

[3] *Electron Transfer from Isolated Molecules to Biomolecules Part 1*, edited by J. Jortner and M. Boxin, Ad. in Chem. Phys., Vol. 106 (John Wiley & Sons, Inc., New York, 1999).

[4] S. H. L. et al, "Ultrafast dynamics and spectroscopy of bacterial photosynthetic reaction centers," in *Advances in Chemical Physics*, Ad. in Chem. Phys., Vol. 121, edited by I. Prigogine and S. A. Rice (John Wiley & Sons, Inc., New York, 2002) p. 1.

[5] B. Albinsson and J. Martensson, J. Photochem. Photobiol. C **9**, 138 (2008).

[6] L. D. Zusman, Chem. Phys. **49**, 295 (1980).

[7] M. Tachiya, J. Phys. Chem. **93**, 7050 (1989).

[8] A. Yoshimori, T. Kakitani, Y. Enomoto, and N. Mataga, J. Phys. Chem. **93**, 8316 (1989).

[9] B. Bagchi and G. R. Fleming, J. Phys. Chem. **94**, 9 (1990).

[10] K. Yoshihara, K. Tominaga, and Y. Nagasawa, Bull. Chem. Soc. Jpn. **68**, 696 (1995).

[11] A. Garg, J. N. Onuchic, and V. Ambegaokar, J. Chem. Phys. **83**, 4491 (1985).

[12] P. Wolynes, J. Chem. Phys. **86**, 1957 (1987).

[13] S. Mukamel, *Principles of Nuclear Optical Spectroscopy* (Oxford, New York, 1994).

[14] R. Kubo and Y. Toyozawa, Prog. Thoer. Phys. **12**, 805 (1954).

[15] Y.-J. Yan, M.Sparpaglione, and S. Mukamel, J. Phys. Chem. **92**, 4491 (1988).

[16] S. Mukamel and Y. J. Yan, Acc. Chem. Res. **22**, 301 (1989).

[17] Y. Hu and S. J. Mukamel, Chem. Phys. **91**, 6973 (1989).

[18] G. C. Walker, E. Akesson, A. E. Johnson, N. E. Levinger, and P. F. Barbara, J. Phys. Chem. **96**, 3728 (1992).

[19] Y. Tanimura and S. Mukamel, J. Phys. Soc. Jpn. **63**, 66 (1994).

[20] Y. Tanimura and S. Mukamel, J. Chem. Phys. **101**, 3049 (1994).

[21] Y. Tanimura and Y. Maruyama, J. Chem. Phys. **107**, 1779 (1997).

[22] D. Egorova, Chem. Phys. **347**, 166 (2008).

[23] D. Egorova, M. F. Gelin, M. Thoss, H. Wang, and W. Domcke, J. Chem. Phys. **129**, 214303 (2008).

[24] M. F. Gelin, D. Egorova, and W. Domcke, J. Chem. Phys. **131**, 124505 (2009).

[25] R. Kapral and G. Ciccotti, J. Chem. Phys. **110**, 8919 (1999).

[26] K. Ando and M. Santer, J. Chem. Phys. **118**, 10399 (2003).

[27] Y. Tanimura and S. Mukamel, Phys. Rev. E **47**, 118 (1993).

[28] Y. Tanimura and S. Mukamel, J. Opt. Soc. Am. B **10**, 2263 (1993).

[29] Y. Tanimura and K. Okumura, J. Chem. Phys. **106**, 2078 (1997).

[30] M. Bixon, J. Jortner, and M. E. Michael-Beyerle, Biochim. Biophys. Acta **1056**, 301 (1991).

[31] K. Ando and H. Sumi, J. Phys. Chem. B **102**, 10991 (1998).

[32] T. Kakitani, A. Kimura, and H. Sumi, J. Phys. Chem. **103**, 3720 (1999).

[33] H. Sumi and T. Kakitani, J. Phys. Chem. B **105**, 9603 (2001).

[34] K. Saito, K. Mukai, and H. Sumi, Chem. Phys. **326**, 221 (2006).

[35] K. Saito and H. Sumi, J. Chem. Phys. **131**, 134101 (2009).

[36] K. Saito, T. Kikuchi, K. Mukai, and H. Sumi, Phys. Chem. Chem. Phys. **11**, 5290 (2009).

[37] J. N. Jean, R. A. Friesner, and G. R. Fleming, J. Chem. Phys. **96**, 5827 (1992).

[38] O. Kühn, V. May, and M. Schreiber, J. Chem.Phys. **101**, 10404 (1994).

[39] L. Hartmann, J. Goychuk, and P. Hänggi, J. Chem. Phys. **113**, 11159 (2000).

[40] R. Egger and C. H. Mak, J. Phys. Chem. **98**, 9903 (1994).

[41] M. Topaler and N. Makri, J. Phys. Chem. **100**, 4430 (1996).

[42] Y. Jung, R. J. Silbey, and J. Cao, J. Phys. Chem. A **103**, 9460 (1999).

[43] J. Cao and Y. Jung, J. Chem. Phys **112**, 4716 (2000).

[44] J. Casado-Pascual, C. Denk, M. Morillo, and R. I. Cukier, J. Chem. Phys. **113**, 11176 (2000).

[45] T. O. Cheche and S. H. Lin, Chem. Phys. **274**, 165 (2001).

[46] B. D. Fainberg and V. A. Gorbunov, J. Chem. Phys. **117**, 7222 (2002).

[47] R. X. Xu, Y. Chen, P. Cui, H. W. Ke, and Y. J. Yan, J. Phys. Chem. A **111**, 9618 (2007).

[48] Q. Shi and E. Geva, J. Chem. Phys. **131**, 034511 (2009).

[49] L. Chen and Q. Shi, J. Chem. Phys. **130**, 134505 (2009).

[50] Q. Shi, L. Chen, G. Nan, R. Xu, and Y. J. Yan, J. Chem. Phys. **130**, 164518 (2009).

[51] K. Ando, J. Chem. Phys. **106**, 116 (1997).

[52] K. Ando, J. Chem. Phys. **114**, 9040 (2001).

[53] K. Ando, J. Chem. Phys. **114**, 9470 (2001).

[54] K. H. Hughes, C. D. Christ, and I. Burghardt, J. Chem. Phys. **131**, 124108 (2009).

[55] C. Venkataraman, A. V. Soudackov, and S. Hammes-Schiffer, J. Chem. Phys. **131**, 154502 (2009).

[56] N. Gayathri and B. Bagchi, J. Phys. Chem. **100**, 3056 (1996).

[57] G. L. Closs, L. T. Calcaterra, N. J. Green, K. W. Penfield, and J. R. Miller, J. Phys. Chem. **90**, 3673 (1986).

[58] C. K. Chan, T. J. DiMagno, L. X. Q. Chen, and J. R. Fleming, Proc. Natl. Acad. Sci. USA **88**, 11202 (1991).

[59] Y. Jia, T. J. DiMango, C. K. Chen, Z. Wang, M. Du, D. K. Hanson, M. Schiffer, J. R. Norris, G. R. Fleming, and M. S. Popov, J. Phys. Chem. **97**, 13180 (1993).

[60] G. R. Fleming and R. V. Grondelle, Phys. Today **47**, 48 (1994).

[61] T. Arlt, S. Schmidt, W. Kaiser, C. Lauterwasser, M. meyer, H. Scheer, and W. Zinth, Proc. Natl. Acad. Sci. USA **90**, 11757 (1993).

[62] B. P. Paulson, H. R. Miller, W. X. Gan, and G. Closs, J. Am. Chem. Soc. **127**, 4860 (2005).

[63] A. Kira, J. Phys. Chem. **85**, 3047 (1981).

[64] H. Pal, Y. Nagasawa, K. Tominaga, and K. Yoshihara, J. Phys. Chem. **100**, 11964 (1996).

[65] H. Nakamura, *Nonadiabatic Transition: Concepts, Basic Theories and Applications* (World Scientific, 2002).

[66] Y. Tanimura, J. Phys. Soc. Jpn. **75**, 082001 (2006).

[67] I. Goychuk and P. Hanggi, Adv. Phys. **54**, 525 (2005).

[68] A. J. L. et al, Rev. Mod. Phys. **59**, 1 (1987).

[69] A. Ishizaki and Y. Tanimura, Chem. Phys. **347**, 185 (2008).

[70] Y. Tanimura and R. Kubo, J. Phys. Soc. Jpn. **58**, 101 (1989).

[71] Y. Tanimura, Phys. Rev. A **41**, 6676 (1990).

[72] Y. Tanimura and P. G. Wolynes, Phys. Rev. A **43**, 4131 (1991).

[73] A. Ishizaki and Y. Tanimura, J. Phys. Soc. Jpn. **74**, 3131 (2005).

[74] R. X. X. et at, J. Chem. Phys. **122**, 041103 (2005).

[75] A. Ishizaki and G. R. Fleming, Proc. Natl. Acad. Sci. U.S.A. **106**, 17255 (2009).

[76] J. Strümpfer and K. Schulten, J. Chem. Phys. **131**, 225101 (2009).

[77] M. Tanaka and Y. Tanimura, J. Phys. Soc. Jpn. **78**, 073802 (2009).

[78] J. Deisenhofer and H. Michel, Science **245**, 1463 (1989).

[79] B. Sakita and K. Yoshikawa, *Quantum Mechanics of Many Freedom Systems by Path Integral Method* (Iwanami, Tokyo, 1986).

[80] L. Accardi and N. Obata, *Foundations of Quantum Probability Theory* (Makinoshoten, Tokyo, 2003).

[81] R. P. Feynman and F. L. Vernon, Ann. Phys. **24**, 118 (1963).

[82] Y. Tanimura and P. G. Wolynes, J. Chem. Phys. **96**, 8485 (1992).

[83] P. G. Wolynes, in *Lectures in the Science of Complexity, SFI Studies in the Sciences of Complexity*, edited by D. Stein (Addison-Weskey Longman, 1989) p. 355.

[84] R. A. Marcus and P. Siders, J. Phys. Chem. **86**, 622 (1982).

[85] T. Takagahara, E. Hanamura, and R. Kubo, Phys. Soc. Jpn. **43**, 802 (1977).

[86] Y. Tanimura, T. Suzuki, and R. Kubo, J. Phys. Soc. Jpn. **58**, 1850 (1989).

[87] T. Steffen and Y. Tanimura, J. Phys. Soc. Jpn. **69**, 3115 (2000).

[88] T. Kato and Y. Tanimura, J. Chem. Phys. **117**, 6221 (2002).

[89] Y. Tanimura and A. Ishizaki, Acc. Chem. Res. **42**, 1270 (2009).

[90] A. O. Caldeira and A. J. Leggett, Ann. Phys. **149**, 374 (1983).

[91] A. J. Leggett, Phys. Rev. B **30**, 1208 (1984).

[92] J. N. Onuchic and P. G. Wolynes, J. Phys. Chem. **92**, 6495 (1988).